JOURNAL OF SOLID STATE CHEMISTRY 22, 423–438 (1977)

Structural Aspects of the Metal–Insulator Transitions in $V_{0.985}Al_{0.015}O_2$

M. GHEDIRA, H. VINCENT, AND M. MAREZIO

Laboratoire de Cristallographie CNRS, 166X, 38042 Grenoble Cedex, France

AND J. C. LAUNAY

Laboratoire de Chimie du Solide du CNRS, Université de Bordeaux I, 351, cours de la Libération, 33405 Talence, France

Received March 26, 1977; in revised form June 6, 1977

The crystal structure of $V_{0.985}Al_{0.015}O_2$ has been refined from single-crystal X-ray data at four temperatures. At 373°K it has the tetragonal rutile structure. At 323°K, which is below the first metal–insulator transition, it has the monoclinic M_2 structure, where half of the vanadium atoms are paired with alternating short (2.540 Å) and long (3.261 Å) V–V separations. The other half of the vanadium atoms form equally spaced (2.935 Å) zigzag V chains. At 298°K, which is below the second electric and magnetic transition, $V_{0.985}Al_{0.015}O_2$ has the triclinic T structure where both vanadium chains contain V–V bonds, V(1)–V(1) = 2.547 Å and V(2)–V(2) = 2.819 Å. At 173°K the pairing of the V(1) chain remains constant: V(1)–V(1) = 2.545 Å, whereas that of the V(2) chain decreases: V(2)–V(2) = 2.747 Å. From the variation of the lattice parameters as a function of temperature it seems that these two short V–V distances will not become equal at lower temperatures. The effective charges as calculated from the bond strengths at 298 and 173°K show that a cation disproportionation has taken place between these two temperatures. About 20% of the V^{4+} cations of the V(1) chains have become V^{3+} and correspondingly 20% of the V^{4+} cations of the V(2) chains have become V^{5+}. This disproportionation process would explain the difference between the two short V–V distances. Also it would explain why the $T \rightarrow M_1$ transition does not take at lower temperatures.

Introduction

At 340°K the vanadium dioxide, VO_2, undergoes a metal–insulator transition with decreasing temperature with a decrease of $\sim 10^5$ in the electrical conductivity (*1*). At the same temperature a drop in the magnetic susceptibility of a factor of ~ 10 is also observed (*2*). Furthermore, the transition is accompanied by a volume change, with the insulating phase being 0.3% less dense than the metallic one (*3*), and by a structural distortion (*4, 5*). The metallic phase has the tetragonal rutile structure (R), while the insulating phase has a monoclinic distorted structure (M_1). At the $R \rightarrow M_1$ transition the V–V distances acrosss the shared edges alternately decrease and increase, from 2.85 to 2.62 and to 3.16 Å, respectively. This is usually interpreted in terms of a transition in which the d electrons have localized into covalent nonmagnetic bonds between two transition-metal atoms so that the final spin state is a singlet. In order to elucidate the $R \rightarrow M_1$ transition the effects of vatious dopants on the electrical, magnetic, and structural properties have been investigated. As pointed out by Pouget *et al.* (*6, 7*) the various cation impurities can be divided into two categories; those which enter the structure as 5+ or 6+, such as Nb, and those which enter the structure as 3+, such as Cr and Al, and

ISSN 0022–4596

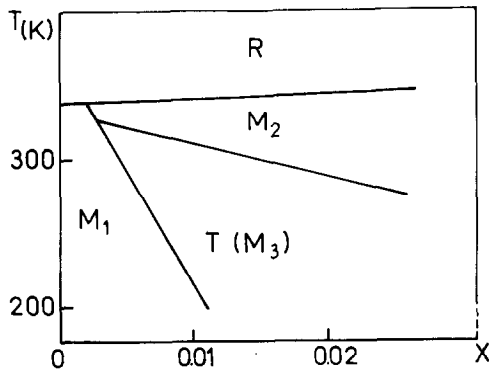

FIG. 1. Phase diagram for $V_{1-x}Cr_xO_2$ as it appears in Ref. (*8*).

produce V^{5+} cations. The first class of cations gives rise to a decrease of the transition temperatures, but below 6.5% of dopant the insulating phases are crystallographically identical to the M_1 phase of pure VO_2. The second class of cations gives rise to an increase of the transition temperatures and leads to complex phase diagrams with several new insulating phases, M_2, T, and M_4, which are crystallographically different from the M_1 phase. These new phases are still rutile like, however, the distortions are markedly different. For instance, in the monoclinic M_1 structure the twofold axis is along the a pseudorutile axis, whereas in the monoclinic M_2 structure it is along the c pseudorutile axis. Since these new phases are stable at concentrations as low as 0.2%, Pouget *et al.* (*6*) suggested that they should be interpreted as possible phases of pure VO_2 whose free energy is only slightly larger than that of the M_1 phase.

Figure 1 shows the phase diagram of the $V_{1-x}Cr_xO_2$ system as obtained by Marezio *et al.* (*8*). At concentrations larger than 0.2% the metal–insulator transition, where the electrical conductivity decreases by a factor of $\sim 10^5$, corresponds to the $R \rightarrow M_2$ crystallographic transition. An abrupt decrease and increase are also observed in the magnetic susceptibility and in the unit-cell volume, respectively. The monoclinic M_2 phase contains two crystallographically independent V sites, which form two sets of chains parallel to the pseudorutile c axis. On one set the V cations are paired into V–V covalent bonds with alternating short (2.54 Å) and long (3.26 Å) V–V separations. On the other set the V cations are not paired, but form equally spaced zigzag chains, the distances being 2.93 Å. Marezio *et al.* (*8*) suggested that these unpaired V cations are in fact localized V^{4+} cations. This was confirmed by the observation of two distinct V^{51} lines in the nuclear magnetic resonance spectrum. Pouget *et al.* (*6*) showed that one line had a Knight shift characteristic of a bonded V–V pair while the other line had a negative Knight shift and a large linewidth characteristic of a site with a localized d electron in an insulator.

By further lowering the temperature a second transition ($M_2 \rightarrow T$) is obtained, and finally for $x < 0.01$ at still lower temperatures, the $T \rightarrow M_1$ transition takes place. In the M_1 structure there is only one set of V cations and as we have seen all of them are paired. For $x < 0.04$ the $M_2 \rightarrow T$ transition is accompanied by an increase of the electrical conductivity by a factor of 2. At the same transition the magnetic susceptibility decreases abruptly and the discontinuity is still visible at $x = 0.06$. A discontinuity is also observed in the lattice parameters (*8, 9*).

The transitional (T) phase was first reported to have a monoclinic symmetry with an arrangement which was quite similar to that of the M_2 phase, that is, with one-half of the V sites paired and the other half unpaired (*8*). However, this arrangement did not explain either the small paramagnetic susceptibility of the T phase, characteristic of a structure with all the V sites paired, or its NMR spectrum. The electric field gradient at the V nuclei, obtained by measuring the quadrupolar splittings in the NMR spectrum, is a very sensitive probe of the local environment of the V sites. The experimental data showed clearly that in the T phase, while one sublattice remained totally paired, the other progressively paired with decreasing temperature. Therefore, at low temperatures in the $V_{1-x}Cr_xO_2$ system all cations should be paired, even at concentrations where the $T \rightarrow M_1$ transition does not take place. Such a behavior cannot be explained if one assigns a monoclinic symmetry to the T phase. In fact, the V cations

corresponding to the zigzag chains lie on the mirror planes of the monoclinic space group and their separation is $>b_M/2$. In order for these sites to pair, the mirror plane and the twofold axis must vanish, which corresponds to lowering the point symmetry from $2/m$ to $\bar{1}$. Accurate X-ray powder data taken on a composition which has the T structure at room temperature showed that some splittings could only be explained with a triclinic cell, and therefore the T phase must have the triclinic symmetry (*10*). With this symmetry the zigzag V sites can freely move and pair progressively with decreasing temperature. The fact that the single-crystal X-ray diffraction effects of two T phases have been shown to have monoclinic symmetry at room temperature for a $V_{0.995}Cr_{0.005}O_2$ sample (*11*) and at 180°K for $V_{0.976}Cr_{0.024}O_2$ (*8*) could be reconciled to the NMR and to powder X-ray diffraction data by assuming that the loss of symmetry on going from the $2/m$ to the $\bar{1}$ point group is associated with twin formation (*6*). The VO_2 and the doped-VO_2 crystals twin severely at the $R \rightarrow M_1$ and the $R \rightarrow M_2$ transitions, respectively. This is due to the loss of symmetry on going from the $4/mmm$ to the $2/m$ point group. Usually the doped-VO_2 crystals are found to be twinned according to the (100), (001), (201), and (20$\bar{1}$) laws (*12*). At the $M_2 \rightarrow T$ transition the symmetry operations (010) and $[010]_{180}$ become possible twin operations. If the obliquity is small, then the X-ray single-crystal measurements will not detect the twinning, and the intensities will have monoclinic symmetry. However, the obliquity is not that small, in fact Villeneuve *et al.* found that for a sample such as $V_{0.99}Cr_{0.01}O_2$ the γ angle opens to 90.24°. Such a value is not compatible with twinning by high-order merohedry and cannot produce the exact superposition of the diffraction effects coming from the two individuals. Therefore, twinning alone does not seem to reconcile the powder data with the two very precise structural refinements of the T phases mentioned above.

Figure 2 shows the phase diagram of the $V_{1-x}Al_xO_2$ system as given by Drillon and Villeneuve (*13, 14*). As we have said earlier Al^{3+} is an impurity which enters the VO_2 structure by producing V^{5+} cations, but has the advantage of not perturbating the magnetic properties of the different phases. Below $x = 0.04$ the phase diagram is quite similar to that of the Cr-doped VO_2 system. The same insulating phases are obtained, that is, M_1, M_2,

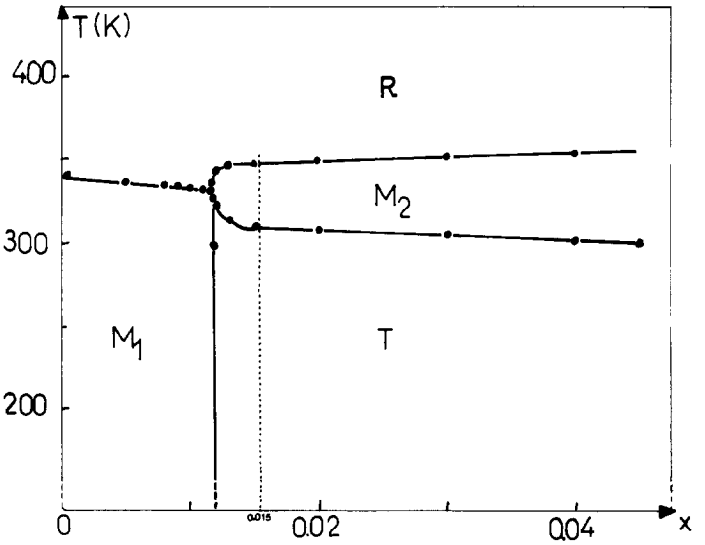

FIG. 2. Phase diagram for $V_{1-x}Al_xO_2$ as given by Drillon in his thesis (*14*).

and T. The only difference between the two systems consists in the fact that in the Al-doped VO_2 the curve between the M_1 and the T phase is almost vertical so that the $T \rightarrow M_1$ transformation has not been observed to take place in any sample. Drillon (*14*) also investigated the electrical and the magnetic properties of this system and found that for $x < 0.045$ the electrical and magnetic behaviors of the $V_{1-x}Al_xO_2$ solid solutions are similar to those of the chromium counterparts.

This paper reports the results of a structural investigation of a $V_{0.985}Al_{0.015}O_2$ single crystal. The twinning, the lattice parameters, and the crystal structures of the R, M_2, and T phases have been determined at different temperatures by X-ray diffraction techniques. The 1.5% composition has been chosen mainly because at toom temperature the crystals have the T structure.

Twinning

The $V_{0.985}Al_{0.015}O_2$ single crystals were prepared by the vapor transport method and analyzed by the atomic absorption method (*14*).

Precession photographs taken with Mo$K\alpha$ radiation showed that $V_{0.985}Al_{0.015}O_2$ single crystals had either the M_2 or the T structure. A small triclinicity could not be detected by the precession geometry. As in the case of the M_2 phase of the $V_{1-x}Cr_xO_2$ system, all crystals were found to be twinned by reticular pseudo-merohedry, controlled by the tetragonal pseudosymmetry of a superlatice obtained from the monoclinic or triclinic cell by the transformation matrix (100/002/0$\bar{1}$0) (*12*). Among all the possible twin laws only those corresponding to (100), (20$\bar{1}$), and (201) were observed in all cases, which meant that the crystals had twinned at the $R \rightarrow M_2$ transition. The X-ray intensities as measured by the automatic diffractometer revealed that these crystals at room temperature had the T structure. Therefore, the additional loss of symmetry occurring at the $M_2 \rightarrow T$ transition had not caused any twinning. As we have seen above, at this transition the (010) plane of symmetry becomes a possible twin law. In the precession photographs all the spots belonging to the two planes **ab** and **bc** were definitely single.

The (100) twin law can be easily detected as it corresponds to a fairly large obliquity ($\sim 1°$) and therefore the spots coming from the two individuals related by this law are well separated. On the contrary, the (20$\bar{1}$) and (201) laws are characterized by a small value of the obliquity, which depends mainly upon the c/a ratio. The individuals twinned by these two operations give reflections either almost exactly superposed on each other for $k = 2n$ or at $(2n'a^*,((2n'' + 1)/2)c^*)$ for $k = 2n + 1$. For instance, the 401 reflection is found to be superposed on the 202 one, whereas the 311 of one individual goes to the $21\frac{3}{2}$ reciprocal node of the other.

Intensity Data Collection

Three small single crystals were ground into spheres 0.18, 0.18, and 0.20 mm in diameter, respectively. Since every crystal was severely twinned, which made its orientation on the automatic diffractometer very difficult, each sphere was first oriented with a precession camera. It was then remounted in order to have within 1° the triclinic a axis along the ϕ axis of the goniostat of a Philips, four-circle, automatic diffractometer equipped with a graphite monochromator and Mo$K\beta$ radiation. The use of the β radiation reduced the intensity of the reflections by a factor of ~ 3, however, its monochromaticity separated the two individuals related by the (100) twin operation at values of θ greater than 15°. Therefore, it made the search for the orientation matrix easier.

The intensity data for the T phase were collected at room temperature and at 173°K. The low temperatures were attained by blowing a cold stream of nitrogen gas directly on the crystal. The integrated intensities, corresponding to one individual, were measured by the following procedure: (1) stationary

crystal–stationary counter technique after maximization of the reflection on the four circles; (2) 1° vertical and horizontal counter slits; (3) the reciprocal lattice region, where the measurements were made, was limited to $\theta > 15°$, and to those reflections whose normal made an angle with the b_T axis greater than 30°. These limitations were necessary in order to separate the spots corresponding to the two individuals related by the (100) twin operation. (4) Only those reflections with $k = 2n + 1$ were measured. This criterion separated the individuals related by the $(20\bar{1})$ and (201) twin operation. (5) The background was measured at $\pm 0.7°$ off the peak maximum along the θ circle. By measuring all those reflections for which $\theta < 35°$, it resulted in 388 and 382 independent reflections with nonzero intensity for the T phase at room temperature and at 173°K, respectively.

TABLE I

OBSERVED NET INTENSITIES (ON AN ARBITRARY SCALE) OF REFLECTIONS WHICH ARE SYMMETRY RELATED IN THE M_2 PHASE, BUT ARE INDEPENDENT IN THE T PHASE

$h\,k\,l$	I_{M2}	I_{T298}	I_{T173}	$h\,k\,l$	I_{M2}	I_{T298}	I_{T173}
1 1 4	13052	11626	15345	5 3 5	3992	3183	3870
1 $\bar{1}$ 4	12847	7055	8050	5 $\bar{3}$ 5	3942	1938	1145
1 1 $\bar{5}$	9921	5499	4680	5 3 7	2886	2400	3255
1 $\bar{1}$ $\bar{5}$	9527	8401	10674	5 $\bar{3}$ 7	2747	1361	1267
1 1 $\bar{6}$	3393	3844	4885	5 7 $\bar{4}$	11191	8650	7635
1 $\bar{1}$ $\bar{6}$	3460	1865	2507	5 $\bar{7}$ $\bar{4}$	10586	5530	5433
1 1 6	4845	5421	7985	7 1 $\bar{2}$	24097	23240	20535
1 $\bar{1}$ 6	4782	2398	2964	7 $\bar{1}$ $\bar{2}$	24000	12165	13691
1 1 8	2685	4482	2820	11 1 2	5941	8206	11529
1 $\bar{1}$ 8	2547	1919	1410	11 $\bar{1}$ 2	5905	3856	3720
1 3 3	20863	14207	15041	11 1 $\bar{3}$	2331	1539	2072
1 $\bar{3}$ 3	20801	13313	14440	11 $\bar{1}$ $\bar{3}$	2308	2655	3500
1 3 $\bar{4}$	19608	13050	12751	11 1 $\bar{4}$	4705	4709	6551
1 $\bar{3}$ $\bar{4}$	19173	13838	15353	11 $\bar{1}$ $\bar{4}$	4665	2643	3400
1 3 5	10383	7885	8904	11 1 $\bar{6}$	1137	1160	1667
1 $\bar{3}$ 5	10887	6439	7040	11 $\bar{1}$ $\bar{6}$	1107	754	1330
1 3 $\bar{6}$	9825	6280	6696	11 3 $\bar{1}$	13897	12120	13137
1 $\bar{3}$ $\bar{6}$	9583	7404	9457	11 $\bar{3}$ $\bar{1}$	14210	6257	16751
1 3 7	5557	4693	6394	11 3 $\bar{3}$	7855	6501	7554
1 $\bar{3}$ 7	5365	2889	3405	11 $\bar{3}$ $\bar{3}$	7835	3728	3687
1 3 $\bar{8}$	3271	1652	1365	11 3 3	5079	6088	7714
1 $\bar{3}$ $\bar{8}$	3127	2993	4208	11 $\bar{3}$ 3	4964	2194	2842
1 5 $\bar{3}$	22218	17963	20552	13 1 $\bar{3}$	3580	4292	6507
1 $\bar{5}$ $\bar{3}$	22106	12922	12353	13 $\bar{1}$ $\bar{3}$	3400	2072	2528
5 1 $\bar{3}$	25339	18952	19207	13 3 $\bar{2}$	5933	5318	5923
5 $\bar{1}$ $\bar{3}$	23467	16610	16613	13 $\bar{3}$ $\bar{2}$	6357	2662	2604
5 1 $\bar{5}$	10336	7428	7389	13 3 2	5606	5983	6698
5 $\bar{1}$ $\bar{5}$	9851	9881	8413	13 $\bar{3}$ 2	5605	2777	2596
5 1 $\bar{6}$	2087	3327	2242	13 3 $\bar{4}$	3797	3447	4442
5 $\bar{1}$ $\bar{6}$	1917	1514	1214	13 $\bar{3}$ $\bar{4}$	3847	2146	2604
5 1 $\bar{7}$	3215	3005	2310	15 1 1	1754	1397	1624
5 $\bar{1}$ $\bar{7}$	3177	4719	3089	15 $\bar{1}$ 1	1890	2803	4280
5 3 3	4263	3119	3320	15 3 $\bar{1}$	3884	3936	4812
5 $\bar{3}$ 3	4303	2535	1967	15 $\bar{3}$ $\bar{1}$	3878	1517	5214
5 3 $\bar{4}$	22535	16576	18172	9 3 $\bar{4}$	8641	6892	8094
5 $\bar{3}$ $\bar{4}$	21901	15293	14509	9 $\bar{3}$ $\bar{4}$	8610	5033	5186

The intensity data of the M_2 phase were collected at 323°K. The high temperature was obtained by blowing a heated stream of nitrogen gas on the crystal. The procedure for the intensity data collection was the same as for the T phase. The total number of independent reflections with nonzero intensity was 229. Each one represented the average of at least two measurements made on two equivalent reflections.

Table I shows the net intensities of some reflections for the M_2, T_{298}, and T_{173} phases, respectively. It can be seen that in the case of the M_2 phase the intensities do contain the mirror plane perpendicular to the b axis, whereas in the other two phases such a plane has vanished, which strongly confirms the triclinicity of these two phases and that the crystal did not twin at the $M_2 \rightarrow T$ transition. The same results were obtained for the other two spheres.

The intensity data for the R phase were collected at 373°K. It was noticed that when the twinned crystal went through the $M_2 \rightarrow R$ transition, it did not coalesce into a single crystal. Consequently, the intensity of equivalent reflections varied over a large range and there were cases for which it varied by more than 50%. It was decided then to assign to each reflection the strongest measured intensity. The measurements were limited to the θ interval 8–35°. This resulted in a total number of 66 independent reflections.

A spherical absorption correction (μR = 0.60) was applied together with the Lorentz-polarization corrections in order to convert the intensities of the four phases into structure factors.

Lattice Parameters

Table II gives the lattice parameters and the unit-cell volume of $V_{0.985}Al_{0.015}O_2$ as a function of temperature from 133 to 373°K. Their values were determined from the same single crystal which had been mounted on the automatic diffractometer for the intensity data collection. The least-squares refinement was

TABLE II

LATTICE PARAMETERS[a] AND VOLUME OF $V_{0.985}Al_{0.015}O_2$ AS A FUNCTION OF TEMPERATURE

T	a	b	c	α	β	γ	V
−140	9.063	5.7476	4.5223	89.99	91.03	89.75	235.53
−130	9.062	5.7479	4.5219	89.99	91.05	89.75	235.50
−120	9.067	5.7481	4.5212	89.99	91.05	89.76	235.60
−110	9.064	5.7488	4.5219	89.99	91.04	89.77	235.57
−100	9.065	5.7492	4.5212	90.00	91.06	89.78	235.59
−90	9.060	5.7502	4.5216	89.99	91.06	89.77	235.52
−80	9.063	5.7499	4.5215	89.99	91.08	89.77	235.56
−70	9.062	5.7505	4.5221	90.00	91.07	89.78	235.60
−60	9.063	5.7523	4.5208	89.99	91.08	89.75	235.66
−50	9.062	5.7531	4.5216	89.98	91.09	89.77	235.69
−40	9.058	5.7546	4.5210	89.99	91.12	89.78	235.61
−30	9.063	5.7542	4.5211	89.98	91.17	89.74	235.72
−20	9.059	5.7568	4.5212	90.00	91.13	89.76	235.73
−10	9.062	5.7578	4.5210	89.99	91.14	89.79	235.82
0	9.063	5.7588	4.5218	89.99	91.16	89.79	235.96
10	9.062	5.7637	4.5212	89.99	91.23	89.79	235.09
22	9.060	5.7721	4.5203	89.99	91.40	89.83	235.33
50	9.060	5.8000	4.5217	90.00	91.85	90.00	237.48
100	9.1092	5.7056	4.5546	90.00	90.00	90.00	236.72

[a] The estimated standard deviation for the lattice parameters is about 1/10 000 and that of the interaxial angles is ±0.01°.

applied to the 2θ values of 18, 18, and 10 reflections for the T, M_2, and R phases, respectively. The zero of the θ– circle was obtained by measuring the θ circle was obtained by measuring the θ and the $-\theta$ values for each reflection. For the M_2 and R phases the lattice parameters were measured only at one temperature, that is, the temperature at which the structure of the two phases was determined. Between room temperature and 100°C with our gas blower attachment the absolute temperature is known within 10°C. This uncertainty did not allow the determination of the lattice parameters of the three phases, T, M_2, and R, close to the transitions.

Structural Refinements

All structure refinements were carried out with the LINEX program together with the f curves for neutral atoms given by Doyle and Turner (*15*). The real and imaginary anomalous dispersion coefficients for vanadium were those given by Cromer and Liberman (*16*). Each observed structure factor was weighted by $w = 1/\sigma^2$, where $\sigma = a$ when $|F| \leqslant 10a$ and $\sigma = 0.1|F|$ when $|F| > 10a$. A different value of a was chosen for each structure. In general it was taken 0.02 times the strongest reflection.

1. T Phase at Room Temperature

For this structure the starting positional and isotropic thermal parameters were deduced from those of the M_2 phase of $V_{0.976}Cr_{0.024}O_2$ (*8*). In the T structure all atoms (two vanadium and four oxygen atoms) are in the general positions. In the first few cycles the scale factor, the secondary extinction coefficient, 18 positional, and six thermal isotropic parameters were varied. After convergence was attained, the R and wR factors were 0.049 and 0.078, respectively. The introduction of the anisotropic temperature factors for all the atoms yielded lower R and wR factors, however, the values of the temperature factors of O(1) and O(4) were negative. This was due to the fact that for the structure factors of the reflections with h and k odd the contributions of O(1) and O(4) were always very small. In fact, the trigonometric part of the structure factor is given by $\cos 2\pi(hx + lz)\cos 2\pi ky$. Since the y values of O(1) and O(4) are approximately 0.25 and 0.75, respectively, this expression is always close to zero. Therefore, in the last cycles of refinement only the vanadium atoms were assigned anisotropic temperature factors whereas those of all the oxygen atoms were kept isotropic. The R and wR factors decreased to 0.034 and 0.047, respectively. The final positional and thermal parameters are listed in Table III.

2. T Phase at 173°K

The starting positional and thermal parameters for the T phase at 173°K were those of the T phase obtained at room temperature. The R and wR factors with all isotropic temperature parameters were 0.052 and 0.077, respectively. These values dropped to 0.041 and 0.060 upon introduction of anisotropic temperature parameters for the vanadium atoms. The final positional and thermal parameters are given in Table IV.

3. M_2 Phase at 323°K

The starting positional and isotropic thermal parameters were those of the M_2 phase of $V_{0.976}Cr_{0.024}O_2$ (*8*). After convergence was attained the R and wR factors were 0.030 and 0.045, respectively. The introduction of anisotropic temperature factors for the vanadium atoms and for O(2) and O(3) reduced the R and wR values to 0.014 and 0.020. The temperature factor of O(1) was kept isotropic because, as in the T structure, this oxygen contributes very little to the measured structure factors, namely, those with $k = 2n + 1$. Its anisotropic temperature parameters were negative after convergence was obtained. The final positional and thermal parameters are given in Table V.

4. R Phase at 373°K

The starting positional and thermal parameters were those obtained for the rutile

TABLE III

POSITIONAL AND THERMAL PARAMETERS FOR THE T PHASE AT 298°K

	x	y	z	U_{11} or U	U_{22}	U_{33}	U_{12}	U_{13}	U_{23}
V(1)	−0.00430(6)	0.72111(24)	−0.00699(10)	0.0084(2)	0.0066(5)	0.0083(3)	−0.0004(2)	0.0023(2)	−0.0007(2)
V(2)	0.23300(5)	−0.00797(14)	0.52695(13)	0.0063(2)	0.0123(6)	0.0052(2)	0.0008(2)	−0.0014(3)	0.0010(2)
O(1)	0.1494(2)	0.2494(6)	0.2979(7)	0.0068(8)					
O(2)	0.3965(2)	0.0008(6)	0.2103(6)	0.0067(9)					
O(3)	0.0998(2)	−0.0009(6)	0.7978(6)	0.0067(8)					
O(4)	0.1463(2)	0.7542(6)	0.2930(7)	0.0064(8)					

TABLE IV

POSITIONAL AND THERMAL PARAMETERS FOR THE T PHASE AT 173°K

	x	y	z	U_{11} or U	U_{22}	U_{33}	U_{12}	U_{13}	U_{23}
V(1)	−0.00681(7)	0.72175(24)	−0.01012(12)	0.0079(3)	0.0069(6)	0.0053(3)	0.0006(3)	0.0008(4)	−0.0021(3)
V(2)	0.23329(6)	−0.01343(20)	0.52519(17)	0.0041(2)	0.0113(7)	0.0040(2)	−0.0009(3)	−0.0004(2)	0.0022(2)
O(1)	0.1511(3)	0.2516(9)	0.3072(10)	0.0073(5)					
O(2)	0.3964(3)	0.0006(8)	0.2135(8)	0.0060(4)					
O(3)	0.1000(3)	0.0000(8)	0.7981(8)	0.0064(5)					
O(4)	0.1461(3)	0.7570(9)	0.2974(8)	0.0079(5)					

TABLE V

POSITIONAL AND THERMAL PARAMETERS FOR THE M_2 PHASE AT 323°K

	x	y	z	U_{11} or U	U_{22}	U_{33}	U_{12}	U_{13}	U_{23}
V(1)	0	0.7189(1)	0	0.0053(1)	0.0054(2)	0.0058(1)	0	0.0014(1)	0
V(2)	0.2312(1)	0	0.5311(1)	0.0040(1)	0.0080(1)	0.0049(1)	0	0.0000(1)	0
O(1)	0.1460(5)	0.2474(1)	0.2865(9)	0.0075(6)					
O(2)	0.6025(12)	0	0.7716(18)	0.0037(7)	0.0031(9)	0.0097(8)	0	0.0017(6)	0
O(3)	−0.0980(12)	0	0.2138(18)	0.0039(10)	0.0040(10)	0.0171(17)	0	−0.0017(10)	0

TABLE VI

POSITIONAL AND THERMAL PARAMETERS FOR THE R PHASE AT 373°K

	x	y	z	U_{11}	U_{22}	U_{33}	U_{12}	U_{13}	U_{23}
V	0	0	0	0.0093(4)	0.0093(4)	0.0066(2)	0.0011(3)	0	0
O	0.3001(4)	0.3001(4)	0	0.0087(6)	0.0087(6)	0.0057(4)	−0.0027(5)	0	0

phase of $V_{0.976}Cr_{0.024}O_2$ at 360°K (*8*). First the structure was refined on an isotropic thermal model. The *R* and *wR* values obtained after convergence were 0.033 and 0.046, respectively. Since in this structure there were no limitations in measuring the *hkl* reflections (in fact the crystal was not twinned), anisotropic temperature factors were introduced for both the vanadium and oxygen atoms. The *R* and *wR* factors dropped to 0.029 and 0.036. The final positional and thermal parameters are given in Table VI.

Results and Discussion

The interatomic distances with their standard deviations, as calculated by the BONDLA program, are given in Tables VII, VIII, and IX for the *T*, M_2, and *R* structures, respectively. Figure 3 shows a projection of the *T* structure on the *ab* plane or the *ac* pseudorutile one.

In the tetragonal rutile structure the oxygen atoms form a close-packed array which is so distorted that it must be considered as intermediate between hexagonal close packed and cubic close packed (*17*). The vanadium atoms occupy half of the octahedral sites. The filled octahedra, as well as the empty ones, form infinite chains parallel to the *c* axis along which the octahedra share the edges perpendicular to the same axis. These chains are linked together by corner sharing. In the oxygen octahedra there are four equivalent V–O distances in a plane and two equivalent ones perpendicular to it. Due to the large distortion of the oxygen array, the four oxygen atoms

TABLE VII

INTERATOMIC DISTANCES IN THE *T* PHASE AT 298 AND 173°K

	298°K	173°K
	V(1) octahedron	
V(1)–O(1)	1.842(3)	1.857(4)
V(1)–O(2)	1.852(3)	1.854(6)
V(1)–O(2)	1.863(3)	1.887(5)
V(1)–O(3)	2.070(3)	2.073(5)
V(1)–O(3)	2.072(3)	2.048(5)
V(1)–O(4)	1.907(3)	1.957(4)
Average	1.934	1.946
O(1)–O(2)	2.727(4)	2.743(6)
O(1)–O(3)	2.706(4)	2.741(7)
O(3)–O(2)	2.883(5)	2.895(6)
O(4)–O(2)	2.711(4)	2.725(6)
O(4)–O(3)	2.668(5)	2.678(7)
O(3)–O(2)	2.887(5)	2.854(7)
O(2)–O(2)	2.705(3)	2.733(6)
O(4)–O(2)	2.728(4)	2.785(6)
O(4)–O(3)	2.665(4)	2.649(6)
O(3)–O(3)	2.598(3)	2.597(5)
O(1)–O(3)	2.700(4)	2.728(6)
O(1)–O(2)	2.736(4)	2.775(7)
	V(2) octahedron	
V(2)–O(1)	1.949(3)	1.947(6)
V(2)–O(1)	1.991(3)	1.996(5)
V(2)–O(2)	2.084(2)	2.056(4)
V(2)–O(3)	1.740(3)	1.744(4)
V(2)–O(4)	1.895(3)	1.846(5)
V(2)–O(4)	1.952(3)	1.940(5)
Average	1.935	1.921
O(1)–O(2)	2.691(4)	2.672(6)
O(4)–O(2)	2.714(4)	2.704(5)
O(1)–O(3)	2.744(4)	2.731(5)
O(4)–O(3)	2.727(4)	2.703(7)
O(1)–O(4)	2.912(5)	2.920(9)
O(1)–O(4)	2.858(5)	2.828(9)
O(1)–O(1)	2.549(4)	2.499(5)
O(1)–O(3)	2.729(4)	2.693(7)
O(4)–O(3)	2.759(4)	2.772(5)
O(4)–O(4)	2.619(4)	2.608(6)
O(4)–O(2)	2.715(4)	2.699(7)
O(1)–O(2)	2.689(4)	2.635(7)
	V–V distances	
V(1)–V(1)	2.547(2)	2.554(2)
V(1)–V(1)	3.226(2)	3.200(2)
V(2)–V(2)	2.819(1)	2.747(2)
V(2)–V(2)	3.005(1)	3.051(2)
V(1)–V(2)	3.556(1)	3.574(1)
V(1)–V(2)	3.427(1)	3.414(1)
V(1)–V(2)	3.454(1)	3.460(1)
V(1)–V(2)	3.506(1)	3.498(1)
V(1)–V(2)	3.676(1)	3.669(1)
V(1)–V(2)	3.405(1)	3.417(1)
V(1)–V(2)	3.457(1)	3.460(1)
V(1)–V(2)	3.652(1)	3.633(1)

TABLE VIII

INTERATOMIC DISTANCES IN THE M_2 PHASE AT 323°K

V(1) octahedron	
V(1)–O(1) × 2	1.831(6)
V(1)–O(2) × 2	1.898(8)
V(1)–O(3) × 2	2.106(5)
Average	1.945
O(1)–O(2) × 2	2.768(8)
O(1)–O(3) × 2	2.724(8)
O(2)–O(3) × 2	2.901(1)
O(1)–O(2) × 2	2.692(10)
O(1)–O(3) × 2	2.647(10)
O(2)–O(2)	2.822(15)
O(3)–O(3)	2.667(15)
Average	2.746
V(2) octahedron	
V(2)–O(1) × 2	1.955(4)
V(2)–O(1) × 2	2.001(4)
V(2)–O(2)	2.068(8)
V(2)–O(3)	1.696(8)
Average	1.946
O(1)–O(1) × 2	2.654(8)
O(1)–O(1)	2.930(1)
O(1)–O(1)	2.870(1)
O(1)–O(2) × 2	2.712(10)
O(1)–O(2) × 2	2.678(8)
O(1)–O(3) × 2	2.702(8)
O(1)–O(3) × 2	2.772(10)
Average	2.736
V–V distances	
V(1)–V(1)	2.540(1)
V(1)–V(1)	3.261(1)
V(2)–V(2)	2.935(1)
V(1)–V(2)	3.533(6)
V(1)–V(2)	3.439(5)
V(1)–V(2)	3.700(6)
V(1)–V(2)	3.422(5)

lying in the plane form a rectangle whose sides differ from each other for about 10%.

In the R phase of $V_{0.985}Al_{0.015}O_2$ at 373°K the two apical V–O distances are 1.933 Å and the four equatorial ones are 1.922 Å, which give 1.927 Å for the average V–O distance. These values are equal to those obtained for the corresponding distances in the R phase of pure VO_2 (*18*) and of $V_{0.976}Cr_{0.024}O_2$ (*8*) at 360°K. The ratio V–O (apical)/V–O (equatorial) varies from one rutile structure to another. In TiO_2 it is 1.016 (*19*), that is, the octahedra are apically elongated, whereas it is 0.990 in CrO_2 (*20*), which is a consequence of apically contracted octahedra. In the pure VO_2 and doped-VO_2 compounds the ratio is the same 1.006.

TABLE IX

INTERATOMIC DISTANCES IN THE R PHASE AT 373°K

V–O × 2	1.933(2)
V–O × 4	1.922(2)
Average	1.926
O–O × 2	2.853(1)
O–O × 2	2.576(3)
O–O × 8	2.726(3)
Average	2.722
V–V across edge	2.853(1)
V–V across corner	3.522(1)

Each cation has 10 nearest cation neighbors; two lie along the c axis, across the two shared octahedral edges, with the remaining eight lying along the body diagonals across the shared corners. The V–V distance across the shared edge is 2.853 Å in the present compound, while it is 2.854 and 2.851 Å in $V_{0.976}Cr_{0.024}O_2$ (*8*) and in pure VO_2 (*18*), respectively. These values are markedly smaller than the corresponding distances in TiO_2 (2.958 Å) (*19*) and in CrO_2 (2.916 Å) (*20*).

The M_2 and T structures consist of four distorted rutile cells (see Fig. 3). The transformation matrix is:

$$\begin{Bmatrix} a \\ b \\ c \end{Bmatrix}_{M_2} = \begin{Bmatrix} 2\,0\,0 \\ 0\,0\,2 \\ 0\,\bar{1}\,0 \end{Bmatrix} \begin{Bmatrix} a \\ b \\ c \end{Bmatrix}_{R} .$$

There are two crystallographically independent V sites in the M_2 structure. With respect to their position in the tetragonal structure the V(1) cations move out of the centers of the oxygen octahedra along the monoclinic b_{M_2} axis in such a way that four of the six V–O distances decrease to an average value of 1.865 Å while the other two expand to 2.106 Å, the overall average being 1.945 Å. The

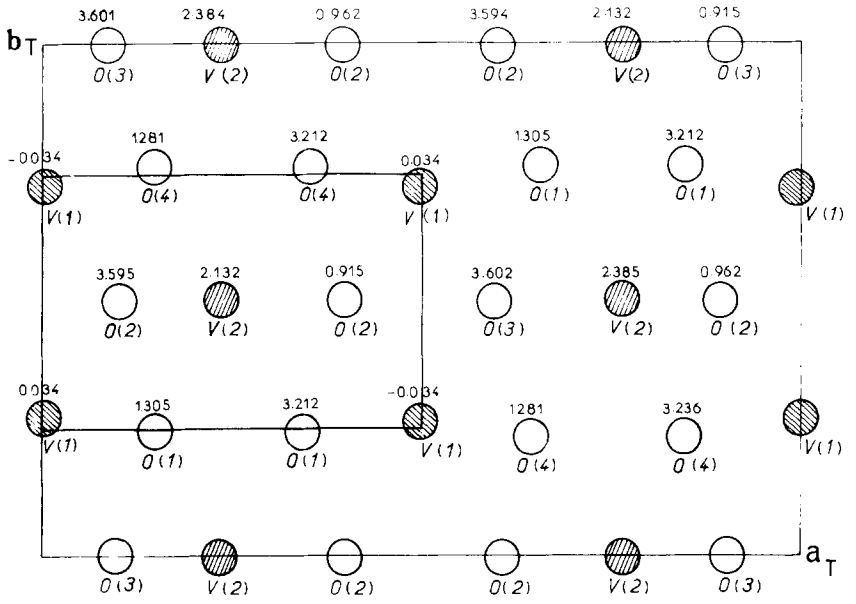

FIG. 3. Projection of the triclinic T phase on the (ab) plane. A rutile cell is outlined for comparison. The heights are shown in angstroms.

oxygen octahedra surrounding the V(2) cations distort in a different way. The four equatorial V–O distances remain relatively equal, whereas the two apical distances expand to 2.068 Å and contract to 1.696 Å, respectively. The average V(2)–O distance is 1.946 Å. The distortions and the average values of the V–O distances are very similar to those found in the M_2 phase of the $V_{0.976}Cr_{0.024}O_2$ compound (*8*). This indicates that the type of impurity does not have a significant effect on the distortion and on the average V–O bond lengths.

On the M_2 structure the V(1) chains are composed of alternate short (2.540 Å) and long (3.261 Å) V–V distances, the average being 2.901 Å. The V(2) chains are comprised of equidistant V atoms (2.935 Å). Since these cations are displaced only in the $(xz)_{M_2}$ plane, a zigzag pattern is obtained. The V(2)–V(2) separation has the same value which one would obtain by interpolating between the Ti–Ti and Cr–Cr distances found in TiO_2 (*19*) and CrO_2 (*20*).

At the $M_2 \rightarrow T$ transition an additional distortion takes place in the structure of $V_{0.985}Al_{0.015}O_2$ as the point symmetry decreases from $2/m$ to $\bar{1}$. This loss of symmetry is needed in order to allow the V(2) cations to form pairs at lower temperatures. In the T structure all atoms are in the general positions and the V(2) cations are free to move out of the $y = 0$ plane and to form covalent bonds as the V(1) cations. On the other hand these cations move out of the twofold axis in such a way that the V(1)–V(1) bond twists around it. The additional distortion of the T structure with respect to the M_2 structure is mainly due to the pairing and twisting of the V(2) and V(1) cations, respectively.

At room temperature in the T structure the V(1)–V(1) distance across the shared octahedral edge is 2.547 as against 2.540 Å in the M_2 phase at 323°K. The slightly larger value found in the T structure is due to the twisting of the bonds. The distortion of the oxygen octahedra around the V(1) cations in the T structure is similar to its counterparts of the M_2 phase. An index of distortion of an oxygen octahedron is given by the standard deviation calculated from the average of the 12 O–O distances. For the V(1) octahedra this index of

distortion decreases from 0.089 to 0.083 on going from the M_2 to the T_{298} structure. There are small individual variations in the six V(1)–O distances between the M_2 and T_{298} structures, however, the overall pattern remains the same, that is, there are four short V(1)–O distances (1.842, 1.852, 1.863, 1.907 Å) and two long ones (2.070, 2072 Å). The average V(1)–O distance is 1.934 Å.

The V(2)-octahedra chains of the T phase are crystallographically different from their counterparts of the M_2 phase. As we have seen, in the latter phase the V(2) cations are equidistant and they form zigzag chains, the V(2)–V(2) separation being 2.935 Å. Since in the T structure the V(2) cations move along the b_T axis, the V(2) chains begin to form alternate short and long V–V distances, 2.819 and 3.005 Å, respectively. Therefore, in the T structure also the V(2) cations pair and twist. This is in a way the bonding pattern found in the M_1 structure, the only difference being that in this structure the V chains are all crystallographically equivalent. The pairing of the V(2) cations induces an appreciable displacement of these cations and as a consequence the oxygen octahedra around these cations increase their distortion on going from the M_2 structure to the T one. The index of distortion increases from 0.086 to 0.095. The average V(2)–O distance has the same value (1.935 Å) as the V(1)–O (1.934 Å).

The T structure as refined at 173°K shows that all the differences in structural details between M_2 and T have increased. For instance, the V(1) atoms have moved further away from the (OyO) position of the M_2 structure and this results in a larger twisting of the V(1)–V(1) pairs. The V(1)–V(1) separation at 173°K is 2.545 Å as against 2.540 Å at 323°K and 2.547 Å at 298°K. The index of distortion of the V(1) oxygen octahedra has further decreased to 0.081. The average V(1)–O distance is 1.946 Å, which is 0.012 Å larger than the value found at room temperature. The V(2) cations are found to have increased their pairing at 173°K. In fact the short V(2)–V(2) distance has decreased to 2.747 from 2.819 Å and the long one has increased to 3.051 from 3.005 Å. The index of distortion of the V(2) oxygen octahedra has increased to 0.106. The average V(2)–O distance is 1.921 Å, which is 0.014 Å smaller than the value found for V(2)–O at room temperature.

Recently Zachariasen (*21*), starting from Pauling's ionic bond strength rules, has developed an empirical formula which allows one, in any oxide of the 3*d* transition metals, to assign a bond strength to each individual bond of the coordination polyhedron. By summing the bond strengths over the anions of the coordination polyhedron one obtains the approximate cation charge of the site, while by

TABLE X

EFFECTIVE CHARGES, V–O AVERAGE DISTANCES, AND V–V SEPARATIONS IN THE R, M_2, T_{298} AND T_{172} STRUCTURES

	R		M_2	T_{298}	T_{173}
Effective charge	3.88	V(1)	3.90	3.96	3.78
		V(2)	3.96	4.00	4.17
V–O average distances	1.926	V(1)	1.945	1.934	1.946
		V(2)	1.946	1.935	1.921
V–V distances across the shared face	2.853	V(1)	2.540 3.261	2.547 3.226	2.545 3.200
		V(2)	2.935 2.935	2.819 3.005	2.747 3.051

summing over the cations one obtains the anion charge. For a vanadium oxide at room temperature Zachariasen gives $d = d(1)\ (1 - 0.171 \ln s)$, where d is the individual interatomic distance, $d(1)$ is the distance corresponding to unit bond strength, and s is the bond strength. The cation charge is given by $\sum s_i$. For a vanadium oxide at room temperature Zachariasen finds that $d(1) = 1.792$ Å. Table X gives the calculated cationic charges for each structure: R, M_2, T_{298}, and T_{173} along with the average V–O distances and the V–V separations across the shared edge. It can be seen that the cationic charge of both V(1) and V(2) in the T structure at 298°K is very close to 4.00+. In the M_2 and R structures the calculated cation charges are V(1) = 3.90+ and V(2) = 3.96+ for the former structure and 3.88+ for the latter structure. These values are all smaller than the expected 4+ value because the single-bond strengths have been obtained by the formula which is valid only at room temperature. Nevertheless, in the M_2 structure the two values are almost the same and they should be normalized to 3.97+ for the V(1) site and 4.03+ for the V(2) site. For the T structure at 173°K the cationic charge of the V(1) site decreases to 3.78+ and that of the V(2) site increases to 4.17+. Their sum is 7.95, which compares very well with the corresponding value (7.96) found at room temperature. The charges seem to indicate that an electron transfer from the V(2) chain to the V(1) chain has taken place between room temperature and 173°K. Some of the V(1) cations have become V^{3+} and some of the V(2) cations V^{5+}.This conjecture is corroborated by the average V–O distances found at 173°K for the V(1) and V(2) sites, 1.946 and 1.921 Å, respectively. Such an analysis of calculating charges from bond distances cannot be carried too far, however, our results clearly favor a model in which about 20% of the V^{4+} cations have disproportionated into V^{5+} and V^{3+}, the former being localized on the V(2) chains and the latter on the V(1) chains.

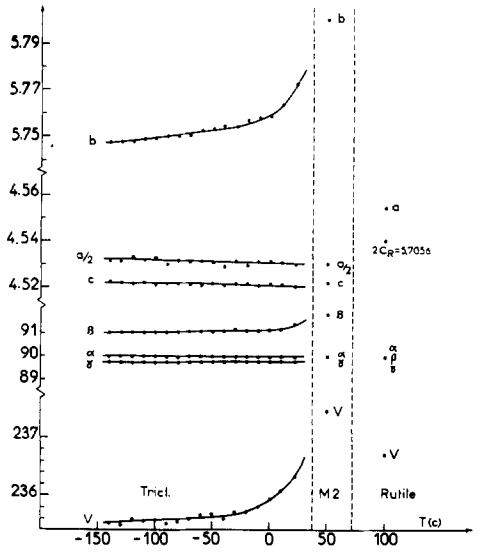

FIG. 4. Lattice parameters and unit-cell volume vs temperature for $V_{0.985}Al_{0.015}O_2$.

Figure 4 shows the variation as a function of temperature of the lattice parameters and the unit-cell volume of the T phase; the lattice parameters and volume of the M_2 and R phase at one temperature are shown for comparison. The a, c, α, γ vary very smoothly between room temperature and −140°C. An anomalous variation is observed instead for the b parameter and for the unit-cell volume. These parameters decrease abruptly for about 30°K below the $M_2 \rightarrow T$ transition. The β angle seems to have a similar behavior within a smaller temperature interval; however, not enough points have been taken which clearly indicate this anomalous decrease after the transition. The abrupt decrease of the b parameter is probably due to the pairing of the V(2) cations. It is likely that the decrease of the V(2)–V(2) separation continues until the variation of the b parameter begins to smooth down with temperature, after which the decrease of the V(2)–V(2) distance would only be that due to the thermal contraction.

In the T structure as determined at 173°K, which is well within the region where the b parameter varies smoothly, the two

separations V(1)–V(1) and V(2)–V(2) are not the same, the former being 2.545 and the latter 2.747 Å. These distances have to be compared with the value of 2.935 Å found in the zigzag chains of the M_2 structure and which compare well with the Ti–Ti separation found in rutile TiO_2. In terms of the logarithmic relation between bond length and bond order suggested by Pauling (*22*) $[r_1 - r_2 = 0.33 \ln (n_1/n_2)]$ where r is the bond length, n is the bond order, and 0.33 is an empirical number, the charge from 2.935 to 2.545 Å for the V(1) chain and that from 2.935 to 2.747 Å for the V(2) chain imply a tripling and a doubling of the bond order in the paired chains over those comprised of localized V^{4+} cations, respectively. This difference in bond order would be compensated by the disproportionation process of the V^{4+} cations into V^{3+} and V^{5+}. It seems probable then that after the V(2)–V(2) bonds have doubled their order the disproportionation begins to take place. This would explain why the $T \rightarrow M_1$ transition does not take place at lower temperatures.

A partial disproportionation of the d electrons of the V^{4+} cations had been suggested by Anderson in 1972 (*23*) in order to reconcile the magnetic properties of the T phase (then M_3) of $V_{0.976}CR_{0.024}O_2$ with the monoclinic symmetry as determined by the X-ray diffraction single-crystal methods. The monoclinic M_3 structure had the same arrangement as the M_2 phase and Anderson proposed that by means of a partial disproportionation of the V^{4+} cations both the xy (σ-like) and the $(x + y)z$ (π-like) orbitals would have been partially occupied in the paired V(1) cations. The V(2) cations of the equally spaced zigzag chains would have had less than one d electron.

Conclusions

It has been shown that in the T phase of the $V_{1-x}Al_xO_2$ system both vanadium chains are paired so as to form covalent bonds between adjacent vanadium cations across the octahedral shared edge. The V–V separations along the two chains are not the same. The V(1) cations, which are already paired in the M_2 structure, form a short distance of 2.545 Å whereas the V(2)–V(2) separation is 2.747 Å. This difference is compensated by a partial disproportionation of the V^{4+} cations into V^{3+} and V^{5+} which takes place after the V(2)–V(2) bonds have doubled their order.

It is difficult at this point to speculate as to what happens with decreasing temperature in the T phase of the $V_{1-x}Cr_xO_2$ system. It seems that the crystallographic details of the two T phases, Cr-doped and Al-doped VO_2, are not exactly the same. The discrepancy between the X-ray powder and the X-ray single-crystal data still remains unexplained in the Cr-doped samples.

Acknowledgments

We wish to acknowledge stimulating discussion with Professor W. H. Zachariasen during his visit to our laboratory.

References

1. F. J. Morin, *Phys. Rev. Lett.* **3**, 34 (1959); and L. Ladd and W. Paul, *Solid State Commun.* **7**, 425 (1969).
2. W. Rudorff, G. Waltyer, and J. Stadler, *Z. Anorg. Allg. Chem.* **297**, 1 (1958); and C. N. Berglund and H. J. Guggenheim, *Phys. Rev.* **185**, 1022 (1969).
3. M. Marezio, P. D. Dernier, D. B. McWhan, and J. P. Remeika, *Mater. Res. Bull.* **5**, 1015 (1970).
4. G. Andersson, *Acta Chem. Scand.* **10**, 623 (1956).
5. J. M. Longo and P. Kierkegaard, *Acta Chem. Scand.* **24**, 420 (1970).
6. J. P. Pouget, H. Launois, T. M. Rice, P. D. Dernier, A. Gossard, G. Villeneuve, and P. Hagenmuller, *Phys. Rev. B* **10**, 1801 (1974).
7. J. P. Pouget, Thèse d'Etat, Orsay (1974).
8. M. Marezio, D. B. McWhan, P. D. Dernier, and J. P. Remeika, *Phys. Rev. B* **5**, 2541 (1972).
9. G. Villeneuve, Thèse d'Etat, Bordeaux (1974).
10. G. Villeneuve, M. Drillon, and P. Hagenmuller, *Mater. Res. Bull.* **8**, 1111 (1973).

11. M. MAREZIO, P. D. DERNIER, D. B. MCWHAN, AND J. P. REMEIKA, unpublished data quoted by (P.D.D.) in the Appendix of (*6*).
12. M. MAREZIO, P. D. DERNIER, AND A. SANTORO, *Acta Crystallogr. A* **29**, 618 (1973).
13. M. DRILLON AND G. VILLENEUVE, *Mater. Res. Bull.* **9**, 1199 (1974).
14. M. DRILLON, Thèse 3ème cycle, Bordeaux (1974).
15. P. A. DOYLE AND P. S. TURNER, *Acta Crystallogr. A* **24**, 390 (1968).
16. D. T. CROMER AND D. LIBERMAN, *J. Chem. Phys.* **53**, 1891 (1970).
17. B. HYDE, private communications (1974).
18. D. B. MCWHAN, M. MAREZIO, J. P. REMEIKA, AND P. D. DERNIER, *Phys. Rev. B* **10**, 490 (1974).
19. S. C. ABRAHAMS AND J. L. BERNSTEIN, *J. Chem. Phys.* **55**, 3206 (1971).
20. P. PORTA, M. MAREZIO, J. P. REMEIKA, AND P. D. DERNIER, *Mater. Res. Bull.* **7**, 157 (1972).
21. W. H. ZACHARIASEN, private communication (1976).
22. L. PAULING, "The Nature of the Chemical Bond," Cornel Univ. Press, Ithaca, N.Y. (1960).
23. P. W. ANDERSON, private communication quoted in Ref. (*8*).